PCCP

PAPER

View Article Online
View Journal | View Issue

Cite this: *Phys. Chem. Chem. Phys.*, 2018, **20**, 15980

Phonon thermal transport in a class of graphene allotropes from first principles†

Xiuxian Yang,[a] Zhenhong Dai, *[a] Yinchang Zhao [a] and Sheng Meng *[bc]

Received 11th February 2018,
Accepted 14th May 2018

DOI: 10.1039/c8cp00987b

rsc.li/pccp

Utilizing first principle calculations combined with the phonon Boltzman transport equation (PBTE), we systematically investigate the phonon thermal transport properties of α, β and γ graphyne, a class of graphene allotropes. Strikingly, at room temperature, a low lattice thermal conductivity κ_L of 21.11, 22.3, and 106.24 W m^{-1} K^{-1} is obtained in α, β and γ graphyne, respectively, which are much lower than that of graphene. We observe contributions from the phonon modes below the specified frequency and find that many optical phonon modes play critical roles in the phonon thermal transport. These optic modes participate in thermal transport, enhancing the phonon scattering process, thus leading to the low κ_L value. Our results provide insights into the thermal transport of graphyne, and forecast its potential applications for thermoelectric and thermal barrier coatings.

I. Introduction

As a result of the discovery of graphene,[1–3] 2D materials have attracted an explosion of interest. Graphene is a 2D single-layer of carbon atoms arranged in the honeycomb lattice structure,[1] and it is reported that graphene-based nanosheets were prepared *via* chemical reduction of exfoliated graphite oxide.[4] Through experimental observation and theoretical calculation, it can be found that graphene exhibits many unusual properties,[5,6] such as quantum spin Hall effects,[7] suppression of weak localization,[8] enhanced Coulomb interactions,[5] and deviation from the adiabatic Born–Oppenheimer approximation.[9] These unusual properties are inseparable from the massless Dirac fermions in graphene,[10] and suggest that graphene is a promising electronic circuit material.[11] Because of the Dirac cone and pseudospin coming from the structural symmetry of graphene, other 2D carbon allotrope materials with similar symmetry may have similar properties. Graphyne is an interesting candidate wherein the atomic structure is obtained by inserting carbon triple bonds (–C≡C–) in graphene while maintaining the 2D hexagonal symmetry, and this new material contains three kinds of structures, namely, α, β and γ graphyne.[12–14] Recently, some members of the graphyne family have successfully been generated in the form of large films on substrates,[15–20] which greatly enhanced the research enthusiasm of people for layer graphyne.

Some prior studies discussed the lattice thermal conductivity κ_L[14, 21, 22] and thermoelectric properties[23–27] of the graphyne family. However, they did not study the intrinsic phonon scattering effects in detail, for example, phonon anharmonic scattering. The κ_L value of a single layer graphene is about 3000–5000 W m^{-1} K^{-1}, and this has been measured through experiments and calculated in theory,[28–30] yet this is much larger than that of α, β and γ graphyne. Therefore, we use the phonon Boltzmann transport equation (PBTE) and first-principle calculations to calculate the κ_L value of these materials. In order to show the accuracy of our results, we also calculated the κ_L value of graphene with the same technical method and compared it with the other results, which was found to be 2962.77 W m^{-1} K^{-1} and fairly consistent with the experimental value of 3000 W m^{-1} K^{-1} at 300 K. Graphene with structural defects (haeckelites) has a significantly decreased κ_L value (250–500 W m^{-1} K^{-1} at 300 K) compared to no-defect graphene.[31] However, it is still larger than graphyne. At the same time, we provide the factors that can determine the κ_L value, such as phonon spectrum, phonon velocities, the relaxation time and weight phase space *etc.* Finally, we obtain the results that the κ_L values of α, β and γ graphyne are 21.11, 22.3, and 106.24 W m^{-1} K^{-1} at room temperature, respectively, which are much lower than that of graphene. We observe the contribution from all phonon modes below the specified frequency, and find that many optical modes play critical roles in the phonon thermal transport.

In this paper, we provided quantitative, physical insights into the harmonic and anharmonic properties that can determine the κ_L of the α, β and γ graphyne, and offer more basic understanding of the lattice thermal transport. The paper is

[a] *School of Opto-electronic Information Science and Technology, Yantai University, Yantai 264005, People's Republic of China. E-mail: zhdai@ytu.edu.cn*
[b] *Beijing National Laboratory for Condensed Matter Physics and Institute of Physics, Chinese Academy of Sciences, Beijing, 100190, People's Republic of China. E-mail: smeng@iphy.ac.cn*
[c] *Collaborative Innovation Center of Quantum Matter, Beijing 100084, People's Republic of China*

† PACS numbers: 65.40.-b, 66.70.-f, 63.20.-e.

organized as follows. In Section II, we briefly discuss the employed theoretical methods and calculation parameters. We present the results of thermal conductivity and further discuss the factors related to the basic thermal properties in Section III, and we provide a summary of our work in Section IV.

II. Methodology

Due to the perfect planar structures of α, β and γ graphyne, we are only interested in phonon–phonon scattering. We used a rigorous method without adjustable parameters to calculate lattice thermal conductivity κ_L and it is effective over a large temperature range of about 200–1000 K. For solving the PBTE, we used the iterative solution (ITS) method, combined with the harmonic (second-order) and anharmonic (third-order) interatomic force constants (IFCs) obtained from the first-principles density functional perturbation theory (DFPT).[32] The κ_L values of the α, β and γ graphyne are isotropic, thus, they can be given by[33–35]

$$\kappa_L^{\alpha\alpha} = \frac{1}{NV}\sum_{\lambda}\frac{\partial f_\lambda}{\partial T}(\hbar\omega_\lambda)\nu_\lambda^\alpha\nu_\lambda^\alpha\tau, \quad (1)$$

where V is the unit cell volume, N is the number of quasi-continuous q points uniformly sampled in the first Brillouin zone (BZ), T is absolute temperature, and f_λ is the distribution function, which depends on the phonon frequency ω_λ, and λ denotes a phonon mode. At the same time, $\hbar$ is the reduced Planck constant, and ν_λ^α and τ are the phonon group velocity of mode λ along the α direction and phonon relaxation time, respectively. When the scattering source is a three-phonon process, it satisfies the conservation of energy and momentum.[36]

Our calculations were performed by the Vienna ab-initio simulation package (VASP)[37] to obtain the optimized structures for these materials. The effect of electronic and ionic convergence criteria on the optimized structures was investigated by using two group parameters, which are 10^{-10} eV and -10^{-8} eV Å^{-1}, as well as 10^{-8} eV and -10^{-6} eV Å^{-1} for these materials, respectively. The structure parameters were found to be nearly identical for both cases, ensuring good convergence for the electronic and ionic relaxation process in the situation of using 10^{-8} eV and -10^{-6} eV Å^{-1} as convergence criteria. The harmonic inter-atomic force constants (IFCs) were obtained by VASP combined with the PHONOPY program[38] using the finite-difference approach within $4 \times 4 \times 1$ supercells and $3 \times 3 \times 1$ k-points for the α, β and γ graphyne, respectively. The anharmonic IFCs were obtained by VASP combined with the thirdorder.py script[33] using the same supercells and Γ-point-only calculations. For the anharmonic IFCs, the interactions were considered to be the third-nearest neighbours of unit cell atoms. The DFT calculations employed the projector augmented wave potential (PAW)[37] to model the ion cores, and a plane-wave basis set with the cutoff energy of 520 eV and the exchange–correlation functional of the generalized gradient approximation (GGA) of the Perdew–Burke–Ernzerhof (PBE)[39] to simulate the valence electrons. The harmonic and anharmonic IFCs are input parameters of the SHENGBTE[33] package, which was employed to solve the PBTE. To acquire accurate results, the effect of the q-grid on the κ_L value was investigated by using the q-grids of $15 \times 15 \times 1$ and $40 \times 40 \times 1$ (recommended by ref. 24). The κ_L value was found to be nearly identical for both cases, ensuring well converged κ_L values for the $15 \times 15 \times 1$ q-grid. In all calculations, we use the fully relaxed optimized lattice structure parameters so that the results can be ensured convergence.

III. Results and discussion

Fig. 1 shows the crystal structures (a–c) and band structures (d–f) of the α, β and γ graphyne, respectively, which are consistent with ref. 12. The black parallelogram in Fig. 1(a–c) represents the primitive cell of α, β and γ graphyne with 8, 18, and 12 atoms, respectively. The atomic structures are obtained by inserting carbon triple bonds (–C≡C–) in graphene, while maintaining the 2D hexagonal symmetry.[12] The α and β graphyne has a Dirac cone as with graphene, while γ graphyne has a direct band gap of about 0.471 eV. We use the harmonic IFCs to calculate the phonon dispersion spectra of these materials in the

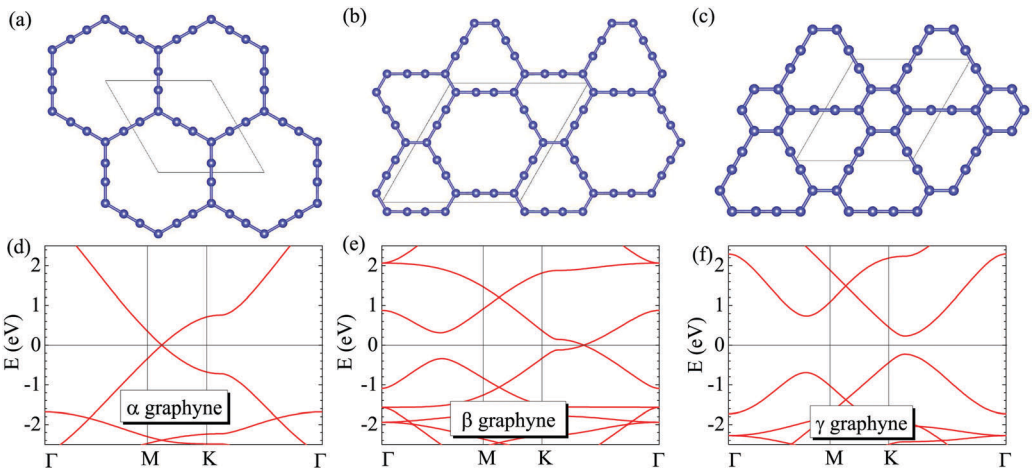

Fig. 1 Crystal structures (a–c) and band structures (d–f) of α, β and γ graphyne, respectively.

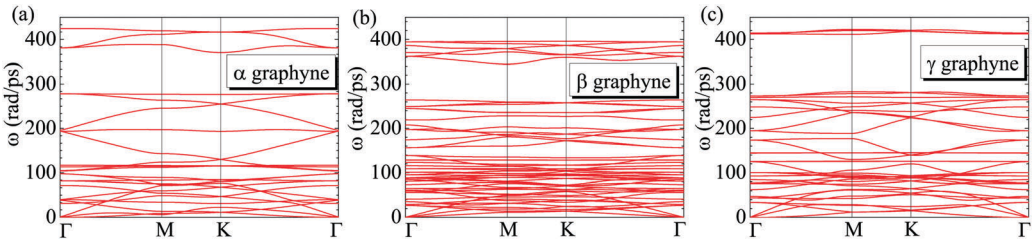

Fig. 2 Phonon dispersion spectra along the high symmetry point in the first Brillouin zone (BZ) of α, β and γ graphyne, respectively.

first Brillouin zone (BZ), and the results are acquired within the linear response framework by adopting DFT as implemented in VASP. The calculated phonon dispersion relations are shown in Fig. 2.

The phonon dispersion spectra of α, β and γ graphyne along the high symmetry point (*Γ*–*M*–*K*–*Γ*) in the first BZ are shown in Fig. 2(a–c), respectively. There are 24, 54, and 36 phonon modes in the primitive cell of these materials, thus it is not necessary to distinguish each phonon mode. Three acoustic modes arise from the *Γ* point, which are the out-of plane mode (ZA), the transverse mode (TA), and the longitudinal mode (LA). For each system, the softest vibration phonon mode is the ZA mode. We can see clearly that these graphynes have no imaginary frequencies, which suggests the thermal stability of these systems. Additionally, around the high symmetry point, the phonon dispersion of many branches is almost linear due to hexagonal structural symmetry. The hexagonal or trigonal crystal symmetry can induce similar characteristics observed in some 2D structures. For instance, nitrogenated holey graphene, metal adatoms decorated silicene, defect-patterned graphene nanomeshes, *etc.*[40–44]

Because of the large excitation energy, low group velocities and phonon occupation of optical modes, the effects of optical modes are usually neglected when calculating the κ_L.[45] However, in some materials, such as $LiMg_2$, the optical modes provide important scattering channels for the acoustic modes, which drastically reduces the κ_L value.[46] Especially in our studied systems, the frequencies of optical modes are comparable with the acoustic modes, and they must be taken into account. The calculated κ_L values of these materials are depicted in Fig. 3(a–c). We represent the κ_L value for ITS calculations by the red solid lines. In our calculation process, the temperature range is from 200 K to 1000 K, and the temperature interval is 50 K. The κ_L values of α, β and γ graphyne are 21.11, 22.3, and 106.24 W m^{-1} K^{-1} at room temperature, respectively. The κ_L value is re-scaled by the factor c/h, where c is the lattice constant along the perpendicular direction (vacuum layer) and h is the thickness of graphyne. Here, c is fixed to be 15 Å and we assume

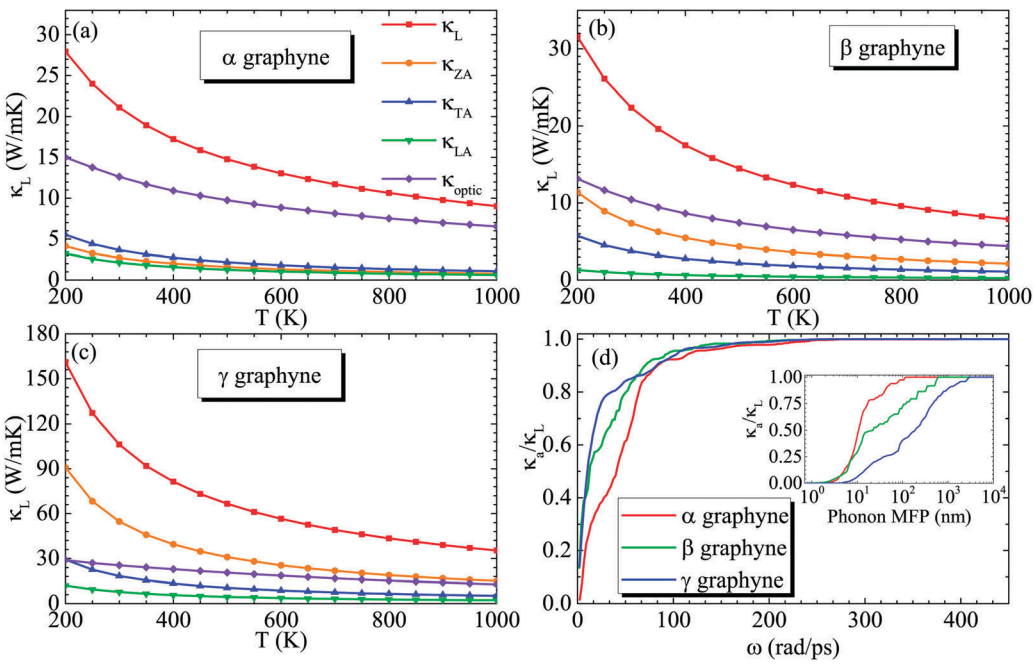

Fig. 3 (a–c) Red curves describe the total κ_L of α, β and γ graphyne as a function of temperature ranging from 200 K to 1000 K, which are obtained by using the iterative method. The solid origin, blue, green and violet curves show the contributions to the total κ_L from the ZA, TA, LA and optic modes, respectively. (d) Accumulative thermal conductivity κ_{accum} scaled by the total κ_L for each system (α, β and γ graphyne) as a function of frequency. The inset picture in (d) shows κ_{accum} of α, β and γ graphyne nanowires along the [100] direction as a function of phonon MFP at room temperature.

h to be 0.34 nm (same as that of graphene).[21,47] Except for γ graphyne, the κ_L values of α and β graphyne are smaller than that of monolayer MoS_2 (34.54 W m^{-1} K^{-1}),[48] black phosphorene (78 W m^{-1} K^{-1})[49] and silicene (26 W m^{-1} K^{-1}).[50] At high temperature, the κ_L values of these materials are considerably low. This is reasonable since at high temperature, more phonons are active, and the Umklapp scattering process will become more critical in the phonon–phonon scattering process and reduce the whole κ_L. In addition, we study the contributions of three acoustic phonon modes, κ_{ZA} (origin cure), κ_{TA} (blue cure), and κ_{LA} (green cure) and the total optic modes κ_{optic} (violet cure) to κ_L, as shown in Fig. 3(a–c).

For γ graphyne, the ZA mode contributes the most to the total κ_L compared with the TA, LA and optic modes, which is similar to graphene, while for α and β graphyne, optic modes contribute the most to κ_L. For example, at 300 K, in γ graphyne, κ_{ZA} contributes almost 51.2% to κ_L, while κ_{TA} and κ_{LA} contribute 17.3% and 7.3%, respectively, hence other contributions (24.2%) are from the optic modes, as shown in Fig. 3(c), which indicates that the ZA mode contributes the most to κ_L and acoustic modes dominate the heat transport. For β graphyne, κ_{ZA}, κ_{TA}, and κ_{LA} contribute 32.8%, 16.4%, and 4.6% to κ_L, respectively, thus other contributions (46.2%) are from the optic modes. This is because except for the similar phonon spectrum and selection rule of γ graphyne and β graphyne with graphene, they also have many more optical modes and a smaller Brillouin zone, and the optical modes contribute much more to heat transport. However, for α graphyne, κ_{TA}, κ_{ZA} and κ_{LA} make contributions of about 17.3%, 12.8% and 10.1% to κ_L, respectively, hence the contribution from the optic modes is almost 59.8%. This is due to the fact that α graphyne has more optical modes and slightly different acoustic modes compared to graphene. As a result, for these materials, the contributions of the optic modes are not negligible, indicating that the optic modes play a critical role in the heat transport, which has a large divergence compared to graphene. For instance, in graphene, the ZA mode has a larger thermal conductivity (about 75% of total κ_L) due to the anomalously large density of states of the ZA mode and a symmetry-based selection rule.[51–53] And, the three acoustic modes are far more significant in comparison with the total contribution of the optical modes, which does not exceed 10% of the total κ_L, as shown in Fig. 2 of ref. 53. To explain the divergence of the heat transport contribution of each phonon mode between graphene and graphyne, firstly, we consider the effect of the symmetry-based selection rule and density of states of the ZA mode for these materials on the heat transport. We find that graphene and graphyne have similar symmetry-based selection rules. Moreover, the ZA modes of α, β and γ graphyne exhibit a parabolic curve trend at the Γ point, which also leads to a large density of states of ZA modes. Therefore, the symmetry-based selection rule and density of states of ZA modes cannot explain this divergence. Secondly, the larger unit cells in α, β and γ graphyne than that of graphene lead to a smaller BZ, which enhances the Umklapp (U) scattering process and results in a smaller total κ_L. However, in graphene, about 60% of both Normal (N) and U three-phonon scattering phase space of ZA phonons is forbidden due to the symmetry-based selection rule. Thirdly, in graphyne, the ZA mode has a smaller frequency (below 11.41, 14.70 and 14.0 for α, β and γ graphyne, respectively) than that of graphene (the frequency of the ZA mode is below 100 rad ps^{-1}, as shown in Fig. 1 in ref. 51), hence leading to smaller phonon group velocities. From eqn (1), we can find that the $\kappa_L \propto \omega$ and $\propto \upsilon$, thus the κ_L of the ZA mode is smaller than that of graphene. Finally, the graphyne phonons with frequency below 100 rad ps^{-1} have many comparative flat optic modes, which have more contributions to the total κ_L due to a large phonon density of states. However, graphene phonons with frequency below 100 rad ps^{-1} have no optic modes, thus the contribution of optic modes can be ignored.

In order to gain more insights into the κ_L of these materials, the accumulative thermal conductivity κ_{accum} was calculated. For clarity, the κ_{accum} values scaled by the total κ_L for each system as a function of frequency at 300 K are shown in Fig. 3(d). The κ_{accum}/κ_L value gives the summed contribution from all modes below the specified frequency. For these materials, phonons with frequency below ∼100 rad ps^{-1} transport more than 90% of the heat, thus we restrict our subsequent discussions to the 0–100 rad ps^{-1} window. From the phonon spectrum in Fig. 2, there are many optic modes in this frequency range. Therefore, these optic modes participate in the phonon scattering and provide more scattering channels. The inset picture describes the contribution from the phonon with the allowed phonon maximum mean-free path (MFP). Also, the κ_{accum} value is normalized to κ_L. It can be seen that the κ_{accum} value keeps increasing as the MFP increases, until reaching the thermodynamic limit, which represents the heat carriers for the longest phonon MFP, and shows values of 105.0, 150.0, and 2979.02 nm for α, β and γ graphyne, respectively. Nanostructures with characteristic length smaller than 10 nm can reduce the total κ_L by 42.0%, 29.5%, and 5.8% for α, β and γ graphyne.

According to eqn (1), the phonon group velocities (V_g), $\frac{\partial f_\lambda}{\partial T}(\hbar\omega_\lambda)$ and phonon relaxation times (τ) are key features in determining κ_L. For these materials, $\frac{\partial f_\lambda}{\partial T}(\hbar\omega_\lambda)$ approaches the Boltzmann's constant k_B. Therefore, $\frac{\partial f_\lambda}{\partial T}(\hbar\omega_\lambda)$ does not influence κ. Fig. 4(a) gives the group velocities *versus* frequency for α, β and γ graphyne within the first BZ, distinguished by the red, blue, and green stars, respectively. Due to 24, 54 and 36 phonon modes in the primitive cell for these materials, respectively, distinguishing each phonon mode is difficult. It can be seen that the group velocities of γ graphyne are larger than other materials, and for the α, β graphyne, the group velocities are almost the same, which is consistent with κ_L. Also, the phonon relaxation time is a main factor in the increase of κ in γ graphyne. The phonon relaxation times consist of both isotopic relaxation times (IRTs) and anharmonic relaxation times (ARTs). The isotopic relaxation times (not shown) are much bigger than the anharmonic relaxation times for these materials, which indicates the negligible influence of isotopic effect on the calculations of κ_L. Thus, the ARTs are responsible for κ_L and depicted in Fig. 4(b) at 300 K. According to Matthiessen's rule, the total scattering rate $1/\tau$ of phonons can

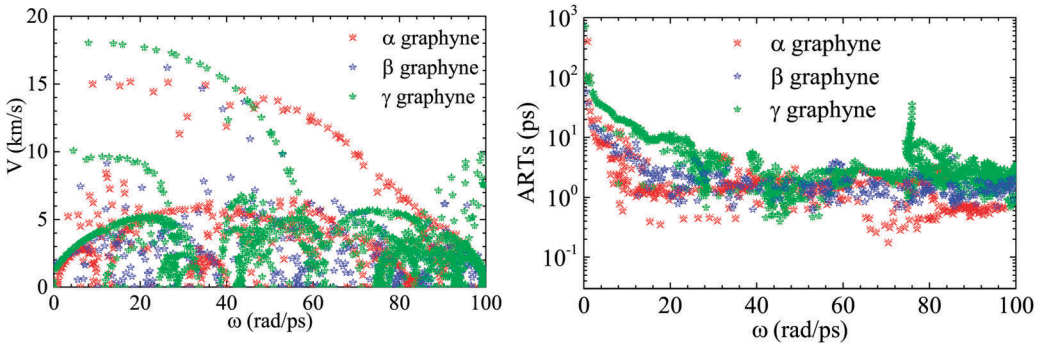

Fig. 4 (a) Phonon group velocities *versus* frequency of α, β and γ graphyne within the first Brillouin zone (BZ). (b) At 300 K, the anharmonic relaxation times (ARTs) of each phonon branch as a function of frequency of α, β and γ graphyne. The red, violet and blue colors represent α, β and γ graphyne, respectively.

be calculated by the isotopic scattering and anharmonic scattering *via* the relation $1/\tau = 1/\tau^{iso} + 1/\tau^{anh}$. The ARTs of γ graphyne are larger than other materials, resulting in a smaller scattering rate and thus large κ_L. The ARTs of α, β graphyne are almost the same, which explains the similar κ_L. Utilizing the phonon group velocities combined with the ARTs, we reveal the intrinsic phonon thermal transport mechanism.

IV. Conclusion

In conclusion, we employed the phonon Boltzmann transport equation (PBTE) theory combined with first-principle calculations to calculate the thermal conductivity κ_L of α, β and γ graphyne, a class of graphene allotropes, which have a Dirac point (α and β graphyne) and a band gap (γ graphyne). Fairly low κ_L values (21.11, 22.3, and 106.24 W m^{-1} K^{-1}) are discovered in these materials. We reveal the intrinsic phonon thermal transport mechanism *via* the phonon group velocities and relaxation times. The low κ_L values of α and β graphyne result from lower group velocities and a stronger anharmonic scattering process compared to that of γ graphyne. In our analysis, lower frequency optic modes participate in the phonon scattering, providing more scattering channels, thus reducing the κ_L value compared to graphene. In addition, the size dependence of lattice thermal transport was investigated, which reveals that the κ_L value can be regulated by the nano device length. In this paper, we emphasized the important role of the harmonic and anharmonic properties in determining heat transport and expect that our work can encourage theoretical and experimental researchers to further investigate graphyne.

Conflicts of interest

There are no conflicts to declare.

Acknowledgements

This research was supported by the National Natural Science Foundation of China under Grant No. 11774396 and No. 11704322, Shandong Natural Science Funds for Doctoral Program under Grant No. ZR2017BA017, the National Key Research and Development Program of China under Grant No. 2016YFA0300902, and the MOST Project of China under Grant No. 2015CB921001, Graduate Innovation Foundation of Yantai University, GIFYTU No. YDZD1810.

References

1 K. S. Novoselov, A. K. Geim, S. V. Morozov, D. Jiang, Y. Zhang, S. V. Dubonos, I. V. Grigorieva and A. A. Firsov, *Science*, 2004, **306**, 666.
2 A. C. Neto, F. Guinea, N. M. Peres, K. S. Novoselov and A. K. Geim, *Rev. Mod. Phys.*, 2009, **81**, 109.
3 S. D. Sarma, S. Adam, E. Hwang and E. Rossi, *Rev. Mod. Phys.*, 2011, **83**, 407.
4 S. Stankovich, D. A. Dikin, R. D. Piner, K. A. Kohlhaas, A. Kleinhammes, Y. Jia, Y. Wu, S. T. Nguyen and R. S. Ruoff, *Carbon*, 2007, **45**, 1558.
5 F. Miao, S. Wijeratne, Y. Zhang, U. C. Coskun, W. Bao and C. N. Lau, *Science*, 2007, **317**, 1530.
6 A. K. Geim and K. S. Novoselov, *Nat. Mater.*, 2007, **6**, 183.
7 D. A. Abanin, P. A. Lee and L. S. Levitov, *Phys. Rev. Lett.*, 2007, **98**, 156801.
8 S. V. Morozov, K. S. Novoselov, M. I. Katsnelson, F. Schedin, L. A. Ponomarenko, D. Jiang and A. K. Geim, *Phys. Rev. Lett.*, 2006, **97**, 016801.
9 X. Lu, X. Luo, J. Zhang, S. Y. Quek and Q. Xiong, *Nano Res.*, 2016, **9**, 3559.
10 K. S. Novoselov, A. K. Geim, S. V. Morozov, D. Jiang, M. I. Katsnelson, I. V. Grigorieva, S. V. Dubonos and A. A. Firsov, *Nature*, 2005, **438**, 197.
11 J. Hass, R. Feng, T. Li, X. Li, Z. Zong, W. A. de Heer, P. N. First, E. H. Conrad, C. A. Jeffrey and C. Berger, *Appl. Phys. Lett.*, 2006, **89**, 143106.
12 B. G. Kim and H. J. Choi, *Phys. Rev. B: Condens. Matter Mater. Phys.*, 2012, **86**, 115435.
13 R. H. Baughman, H. Eckhardt and M. Kertesz, *J. Chem. Phys.*, 1987, **87**, 6687.
14 Y. Zhang, Q. Pei and C. Wang, *Comput. Mater. Sci.*, 2012, **65**, 406.

15 G. Li, Y. Li, H. Liu, Y. Guo, Y. Li and D. Zhu, *Chem. Commun.*, 2010, **46**, 3256.
16 F. Diederich and M. Kivala, *Adv. Mater.*, 2010, **22**, 803.
17 K. Tahara, Y. Yamamoto, D. E. Gross, H. Kozuma, Y. Arikuma, K. Ohta, Y. Koizumi, Y. Gao, Y. Shimizu, S. Seki, K. Kamada, J. S. Moore and Y. Tobe, *Chem. – Eur. J.*, 2013, **19**, 11251.
18 B. Wu, M. Li, S. Xiao, Y. Qu, X. Qiu, T. Liu, F. Tian, H. Li and S. Xiao, *Nanoscale*, 2017, **9**, 11939.
19 Z. Jia, Z. Zuo, Y. Yi, H. Liu, D. Li, Y. Li and Y. Li, *Nano Energy*, 2017, **33**, 343.
20 C. Zhu, A. Rives, C. Duhayon, V. Maraval and R. Chauvin, *J. Org. Chem.*, 2017, **82**, 925, pMID: 27973771.
21 Y. Jing, M. Hu, Y. Gao, L. Guo and Y. Sun, *Int. J. Heat Mass Transfer*, 2015, **85**, 880.
22 J. Wang, A.-J. Zhang and Y. Tang, *J. Appl. Phys.*, 2015, **118**, 195102.
23 P. H. Jiang, H. J. Liu, L. Cheng, D. D. Fan, J. Zhang, J. Wei and J. H. Liang, ArXiv e-prints, arXiv:1608.01877 [cond-mat.mes-hall], 2016.
24 X. Tan, H. Shao, T. Hu, G. Liu, J. Jiang and H. Jiang, *Phys. Chem. Chem. Phys.*, 2015, **17**, 22872.
25 H. Sevinçli and C. Sevik, *Appl. Phys. Lett.*, 2014, **105**, 223108.
26 T. Ouyang and M. Hu, *Nanotechnology*, 2014, **25**, 245401.
27 X.-M. Wang, D.-C. Mo and S.-S. Lu, *J. Chem. Phys.*, 2013, **138**, 204704.
28 A. A. Balandin, S. Ghosh, W. Bao, I. Calizo, D. Teweldebrhan, F. Miao and C. N. Lau, *Nano Lett.*, 2008, **8**, 902.
29 S. Ghosh, I. Calizo, D. Teweldebrhan, E. P. Pokatilov, D. L. Nika, A. A. Balandin, W. Bao, F. Miao and C. N. Lau, *Appl. Phys. Lett.*, 2008, **92**, 151911.
30 Z. G. Fthenakis and D. Tománek, *Phys. Rev. B: Condens. Matter Mater. Phys.*, 2012, **86**, 125418.
31 Z. G. Fthenakis, Z. Zhu and D. Tománek, *Phys. Rev. B: Condens. Matter Mater. Phys.*, 2014, **89**, 125421.
32 S. Baroni, S. De Gironcoli, A. Dal Corso and P. Giannozzi, *Rev. Mod. Phys.*, 2001, **73**, 515.
33 W. Li, J. Carrete, N. A. Katcho and N. Mingo, *Comput. Phys. Commun.*, 2014, **185**, 1747.
34 M. Omini and A. Sparavigna, *Phys. Rev. B: Condens. Matter Mater. Phys.*, 1996, **53**, 9064.
35 A. Ward and D. A. Broido, *Phys. Rev. B: Condens. Matter Mater. Phys.*, 2010, **81**, 085205.
36 J. M. Ziman, *Electrons and phonons: the theory of transport phenomena in solids*, Oxford University Press, 1960.
37 G. Kresse and D. Joubert, *Phys. Rev. B: Condens. Matter Mater. Phys.*, 1999, **59**, 1758.
38 A. Togo, F. Oba and I. Tanaka, *Phys. Rev. B: Condens. Matter Mater. Phys.*, 2008, **78**, 134106.
39 J. P. Perdew, K. Burke and M. Ernzerhof, *Phys. Rev. Lett.*, 1996, **77**, 3865.
40 H. S. Sahin and S. Ciraci, *Phys. Rev. B: Condens. Matter Mater. Phys.*, 2011, **84**, 035452.
41 H. S. Sahin, S. Cahangirov, M. Topsakal, E. Bekaroglu, E. Akturk, R. T. Senger and S. Ciraci, *Phys. Rev. B: Condens. Matter Mater. Phys.*, 2009, **80**, 155453.
42 H. Sahin and F. M. Peeters, *Phys. Rev. B: Condens. Matter Mater. Phys.*, 2013, **87**, 085423.
43 H. Åžahin and S. Ciraci, *J. Phys. Chem. C*, 2012, **116**, 24075.
44 Y. Zhao, Z. Dai, C. Lian and S. Meng, *RSC Adv.*, 2017, **7**, 25803.
45 S. Jandl, J. L. Brebner and B. M. Powell, *Phys. Rev. B: Condens. Matter Mater. Phys.*, 1976, **13**, 686.
46 O. Pavlic, W. Ibarra-Hernandez, I. Valencia-Jaime, S. Singh, G. Avendaño-Franco, D. Raabe and A. H. Romero, *J. Alloys Compd.*, 2017, **691**, 15.
47 A. A. Balandin, S. Ghosh, W. Bao, I. Calizo, D. Teweldebrhan, F. Miao and C. N. Lau, *Nano Lett.*, 2008, **8**, 902, pMID: 18284217.
48 B. Peng, H. Zhang, H. Shao, Y. Xu, X. Zhang and H. Zhu, *Ann. Phys.*, 2016, **528**, 504.
49 A. Jain and A. J. McGaughey, *Sci. Rep.*, 2015, **5**, 8501.
50 X. Gu and R. Yang, *J. Appl. Phys.*, 2015, **117**, 025102.
51 L. Lindsay, W. Li, J. Carrete, N. Mingo, D. A. Broido and T. L. Reinecke, *Phys. Rev. B: Condens. Matter Mater. Phys.*, 2014, **89**, 155426.
52 S. Kajita, H. Washizu and T. Ohmori, *Phys. Rev. B: Condens. Matter Mater. Phys.*, 2010, **82**, 115424.
53 L. Lindsay, D. A. Broido and N. Mingo, *Phys. Rev. B: Condens. Matter Mater. Phys.*, 2010, **82**, 115427.